EVS27
Barcelona, Spain, November 17-20, 2013

Thermal Impedance Spectroscopy for Li-Ion Batteries with an IR Temperature Sensor System

Peter Keil[1], Katharina Rumpf[1], Andreas Jossen[1]
[1] *Institute for Electrical Energy Storage Technology (Technische Universität München), Arcisstr. 21, 80333 Munich, Germany, peter.keil@tum.de*

Abstract

Thermal impedance spectroscopy (TIS) is a non-destructive method for characterizing thermal properties of entire battery cells. Heat capacity, thermal conductivity and heat exchange with environment are determined by an evaluation of the heat transfer behavior of the battery. TIS measurements are usually conducted with contact-based temperature sensors, such as thermocouples or thermistors, which show drawbacks at higher convection rates and higher temperature differences between battery and environment.

To elude drawbacks in these kinds of sensors, an infrared-based temperature sensor system for battery surface temperature measurements is implemented. TIS measurements are conducted with this sensor system and with conventional, contact-based temperature sensors. Accuracy and reliability of thermal parameter identification is analyzed for the different sensor systems. Moreover, thermal parameters are identified for different cylindrical 18650 Li-ion cells with capacities between 1.1 Ah and 2.7 Ah.

The comparison of different types of temperature sensors shows that contact-based sensors underestimate surface temperatures even at low temperature differences to environment. This causes an error in thermal parameter identification. The TIS measurements performed with contact-based sensors show divergence of 20 - 60 % for heat capacity, 30 - 70 % for thermal conductivity and 20 - 60 % for convective heat exchange with environment.

With our IR temperature sensor system, parameter identification is performed for different batteries. Resulting values for specific heat capacity are in a range between 900 and 1020 J/kgK and thermal conductivities in radial direction lies between 3.1 and 3.6 W/mK.

Our investigations show that IR-based temperature sensors are an effective progression for TIS measurements and improve quality of parameter identification at low cost. Moreover, discrepancies mentioned in TIS literature can be explained by our findings.

Keywords: lithium battery, battery model, modeling, thermal management, materials

1 Introduction

Temperature influences many attributes of Li-ion batteries, such as efficiency, usable capacity, aging, and safety [1]. Consequently, a good knowledge of thermal battery parameters is essential for the development of battery systems for electric vehicles. Conventional techniques for the identification of heat capacity and thermal conductivity are mainly based on expensive measurement devices, such as calorimeters, or require a destruction of the battery, such as the xenon-flash method [2].

Barsoukov et al. [3] introduced thermal impedance spectroscopy (TIS) as an alternative, non-destructive method for characterizing thermal properties of entire battery cells. Heat capacity, thermal conductivity, and heat exchange with the environment can be determined without the use of a calorimeter and destruction of the cell. To ascertain the thermal characteristics of a battery, sinusoidal heat excitation is applied to the battery. At the same time, transient battery temperature is measured. In [3], heat excitation is performed with a heating band wound around a cylindrical cell. Evaluating heat transfer behavior for different excitation frequencies yields a characteristic thermal impedance spectrum. This spectrum exhibits the complete thermal characteristics of the battery in question [3]. Schmidt et al. [4] and Fleckenstein et al. [5] have enhanced the TIS method by using internal irreversible losses of the battery instead of an external heating band to induce sinusoidal heat generation.

All TIS publications presented have in common that thermocouples were used for temperature measurements. As these sensors belong to the category of contact-based sensors, they have a major drawback: Only one side of the sensor is in contact with the battery's surface, whereas the back side interacts with the environment [6]. Radiation and convection at the back side of the sensor causes the sensor's temperature to diverge from the battery's surface temperature. This divergence increases with intensified convection that occurs either with larger differences between battery and environment temperature or with forced air flow around the battery. In Figure 1, a thermal image shows the difference between sensor temperature and the battery's surface temperature using a thermocouple sensor. Although the battery temperature of 23.6 °C is only 4 °C above ambient temperature T_∞, the temperature of the sensor tip (23.2 °C) exhibits a difference of -0.4 °C.

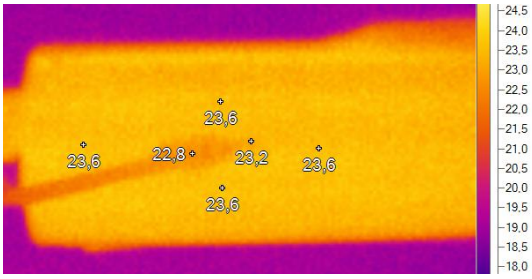

Figure 1: Thermal image of a thermocouple sensor attached to a heated cylindrical battery, illustrating differences between surface and sensor temperature

Figure 2 shows surface temperatures measured for a cell heated with a rectangular current profile consisting of charge and discharge periods which alter every 10 s. An increasing temperature divergence between an infrared (IR)-based thermopile sensor, a thermocouple, and a PT1000 thermistor is evident. The PT1000 sensor has a plane shape of 2 mm x 5 mm, which leads to a weak thermal contact to the cell's cylindrical surface. The differences of thermocouple and PT1000 sensor data demonstrate the inexpediency of contact-based sensors for surface temperature measurements.

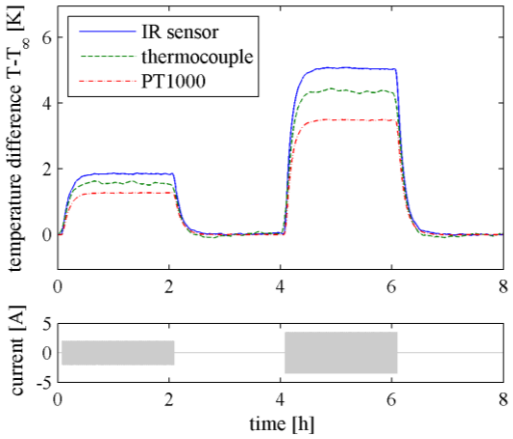

Figure 2: Measurement of temperature increase of a Li-ion battery (2 Ah) heated 2 hours with rectangular pulse current profiles (10 s charge / 10 s discharge)

To improve thermal parameter identification for Li-ion batteries, TIS measurements with a radiation-based sensor system are presented in this article. The process of data evaluation for TIS measurements is explained for cylindrical cells. A comparison of results obtained with different temperature sensors demonstrates the advantages of contact-free temperature measurement. Using the IR-based thermopile sensor system, thermal parameters are identified and compared for different types of 18650 Li-ion batteries. Repeated measurements at varied rates of convection show the reliability of this thermal battery parameter identification technique.

2 Method

Impedance spectroscopy (IS) is a general term for small-signal measurements of linear electrical response analyses to yield information about the physicochemical properties of a system [7]. Usually, a single-frequency current or voltage is applied to the system. Measuring the phase shift and amplitude of the resulting voltage or current, respectively, yields an impedance value for the applied frequency [8].

In contrast to conventional IS analyses, TIS analysis examines the thermal response of a system instead of an electrical response. Evaluating the temperature response T to a specified heat excitation Q yields a characteristic thermal impedance value. In the following sections, the basic principles of TIS are explained. Firstly, thermal impedance is defined. Moreover, the applied method of heat excitation and the IR-based temperature measurement is presented. The impedance values are derived from measurement data and the resulting impedance spectrum is used for a model-based parameter identification that shows the heat capacity, thermal conductivity and heat exchange coefficient for convective heat transfer.

2.1 Thermal Impedance Definition

To describe the heat transfer behavior of a battery for a certain frequency f, a thermal impedance Z_{th} is used. This impedance, representing the temperature response $T(\omega t)$ to a heat excitation $Q(\omega t)$, calculates in the frequency domain as:

$$Z_{th}(\omega t) = \frac{T(\omega t)}{Q(\omega t)} \quad \text{with} \quad \omega = 2\pi f \qquad (1)$$

For a sinusoidal heat excitation, equations (2)-(4) show the calculation of the thermal impedance.

$$Q(\omega t) = \hat{Q} \cdot e^{j(\omega t + \varphi_Q)} \qquad (2)$$

$$T(\omega t) = \hat{T} \cdot e^{j(\omega t + \varphi_T)} \qquad (3)$$

$$Z_{th}(\omega t) = \frac{\hat{T} \cdot e^{j(\omega t + \varphi_T)}}{\hat{Q} \cdot e^{j(\omega t + \varphi_Q)}} = \frac{\hat{T}}{\hat{Q}} \cdot e^{j(\varphi_T - \varphi_Q)} \qquad (4)$$

As heat conduction is rather slow, only frequencies in the millihertz and sub-millihertz range provide meaningful information. Thus, TIS measurements are usually performed in the time domain instead of the frequency domain. For this reason, impedances Z_{th} are derived from a calculation of amplitude ratio ($\hat{T}/\hat{Q}$) and phase delay ($\Delta\varphi = \varphi_T - \varphi_Q$). Thermal impedances for different frequencies result in a characteristic impedance spectrum.

2.2 Heat Generation

To obtain Z_{th}, a sinusoidal heat flow $Q(t)$ has to be applied to the battery. Preferably, this is performed by using irreversible losses of the battery itself that provoke internal heat generation. Applying a sinusoidal current to the battery would cause a charge and a discharge half cycle, which both last up to several minutes and hours for low frequencies in the millihertz and sub-millihertz range. Consequently, the battery´s state of charge changes considerably. Charging or discharging a Li-ion battery is always united with reversible heat generation [9], which would distort the required sinusoidal heat generation. This undesired side-effect is eliminated by using an alternating charge and discharge carrier that is modulated with the frequency f. Figure 3 illustrates the method in which current profiles for our TIS measurements are com-

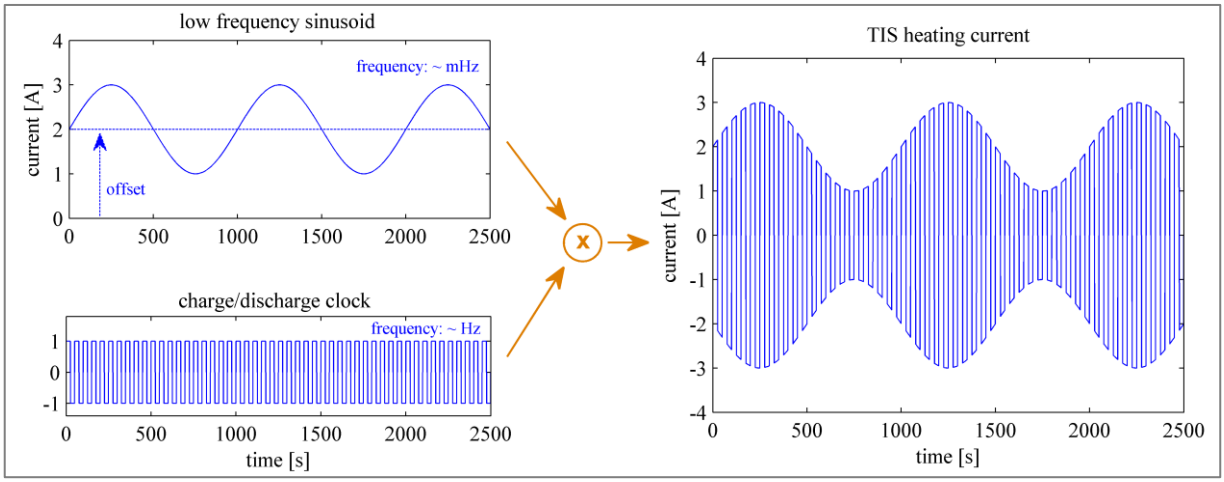

Figure 3: Composition of heating currents for TIS experiments

posed. A low-frequency sinusoid provides the required test frequency in the range of millihertz or microhertz. This signal is multiplied with an alternating, rectangular profile to switch between charge and discharge periods every 3 s. Thus, the battery's state of charge remains constant, while at the same time a sinusoidal heat generation can be achieved. An offset in the low frequency sinusoid signal leads to a permanent generation of heat losses. This prevents the battery from cooling down to environment temperature, which might disproportionately attenuate heat exchange due to natural convection.

Table 1 shows the parameters of the applied heating currents. The first heating signal is repeated for a longer time to heat up the battery and establish steady-state conditions. As lower frequencies provide a better signal to noise ratio, fewer repetitions are performed.

The entire heating profile is applied to the battery by a BaSyTec battery test system. Figure 4a and Figure 4b show current and voltage measurements of a TIS experiment.

Table 1: Parameter set for TIS heating currents

Frequency	Offset	Amplitude	Repetitions
4.0 mHz	2.0 A	1.0 A	30
2.0 mHz	2.0 A	1.0 A	9
1.0 mHz	2.0 A	1.0 A	6
0.4 mHz	2.0 A	1.0 A	4
0.2 mHz	2.0 A	1.0 A	4
0.1 mHz	2.0 A	1.0 A	3
0.04 mHz	2.0 A	0.8 A	3

2.3 Heat Loss Calculation

Electrical measurement values, such as current, voltage, charge balance (Ah), and energy balance (Wh), are recorded by the battery test system every 500 ms. Charge and energy balance are updated inside the test system every few milliseconds. From the recorded data, heat losses can be calculated after the measurement. For each pair of charge and discharge pulses, energy loss is observed. An interpolation between measurement points assures that the evaluated end point of a pulse pair has the same charge content as the start point. In this case, the energy loss equals the difference in Wh balance between start and end point. Dividing these energy losses by the duration of the pulse pair yields the required heating power. As duration of pulse pairs is short compared to an entire period of the low-frequency sinusoid, the heat calculation provides a smooth and accurate heat generation curve, which can be seen in Figure 4c.

2.4 Temperature Measurement

In addition to the heating power curve, a surface temperature curve is required as the second input for thermal impedance calculation. To overcome drawbacks of contact-based temperature sensors, IR thermopile sensors are used for surface temperature measurement. The lower absolute accuracy of radiation-based sensors compared to contact-based sensors is only of minor importance, as the TIS method evaluates only temperature differences, which can be reproduced precisely. The PerkinElmer A2TMPI 334 sensor employed is

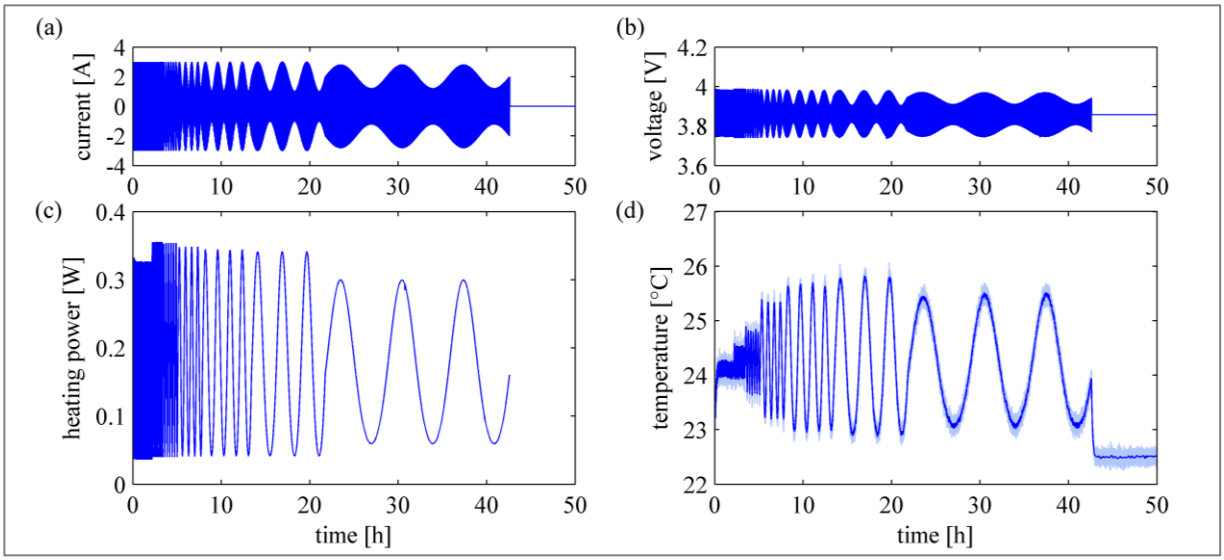

Figure 4: Measurement data of a TIS experiment comprising (a) current, (b) terminal voltage, (c) computed heat losses, and (d) surface temperature (raw and median-filtered thermopile data)

shown in Figure 5 with and without isothermal copper housing. The isothermal housing prevents uneven temperature distribution along the sensor casing, which might deteriorate the highly sensitive measurement of captured heat radiation.

Figure 5: IR thermopile sensor with and without isothermal housing

The sensor has an integrated data processing unit and covers a temperature range from -20 °C to 100 °C. It converts thermopile voltages of a few microvolts into an output voltage between 0 V and 5 V. The output voltage is digitalized by an analog-to-digital converter and the result is transmitted by a microcontroller system via USB interface. Temperature data is recorded synchronously by the battery test system. Figure 4d shows raw and median-filtered surface temperature values.

2.5 Impedance Calculation

As formulated in equation (4), thermal impedance Z_{th} has to be calculated from surface temperature and heat losses. Firstly, measurement data is subdivided into sections for each frequency. As there is always a certain transition period when changing the heating frequency, the first third of measurement data for each frequency is discarded. For the remaining two thirds, surface temperature curve and heat losses are approximated by an analytical expression. This curve fitting is performed with a non-linear least-squares optimization routine. Figure 6 shows that both curves cannot be approximated properly with a single sinusoid, expressed by:

$$y(t) = O + A\sin(2\pi f \cdot t + \alpha) \qquad (5)$$

with offset O, amplitude A, and phase angle α. Fast Fourier transform (FFT) analyses revealed that the intensity of the second harmonic always accounts for up to 10% of the intensity of the fundamental frequency. This observation is in accordance with FFT results presented in [5]. Therefore, the following combination of two sinusoids with fundamental and double frequency is employed for approximation:

$$y(t) = O + A_1\sin(2\pi f \cdot t + \alpha_1) + A_2\sin(4\pi f \cdot t + \alpha_2) \qquad (6)$$

with fundamental frequency f, offset O, amplitudes A_1, A_2, and phase angles α_1, α_2. This expression leads to an excellent approximation of measurement curves (see Figure 6).

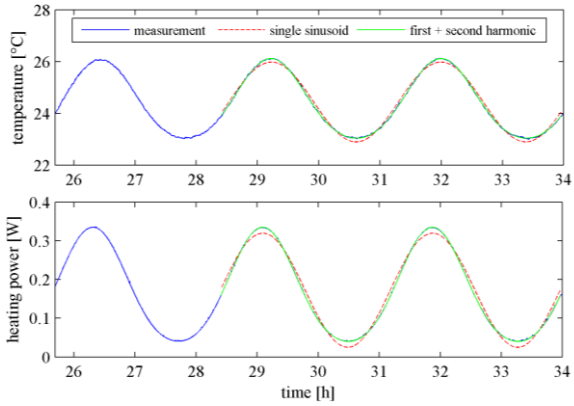

Figure 6: Approximation of the last two thirds of experimental data with a single frequency sinusoid and with a combination of two sinusoids (first + second harmonic)

Following this data processing, the ratio of A_1 values and the difference of α_1 values from heating and temperature curves represent amplitude and phase of the thermal impedance Z_{th} for each fundamental frequency.

$$Z_{th,1}(\mathrm{j}\omega) = \frac{A_{1,T}}{A_{1,P}} \cdot \mathrm{e}^{\mathrm{j}(\alpha_{1,T}-\alpha_{1,P})} \qquad (7)$$

This impedance calculation can also be performed for the second harmonics by evaluating the corresponding pairs of A_2 and $\alpha_2$values.
The impedance spectrum obtained from fundamental frequencies serves as the basis for thermal parameter identification; the spectrum obtained from harmonics is used for consistency checks.

2.6 Thermal Battery Model

To extract thermal battery parameters from a measured impedance spectrum, a thermal model of the battery is necessary. This model reproduces the effects of heat capacity, thermal conductivity, heat exchange with environment, and internal losses generation. Transient simulation is then used to calculate an impedance spectrum for the battery model, which is subsequently employed for parameter identification.
Since all our TIS experiments are performed with cylindrical 18650 batteries inside a temperature chamber, homogeneous environment temperatures can be assumed. As generated heat losses inside the cells are rather low (< 0.5 W) and the temperature increase during TIS experiments accounts only for a few °C (see Figure 4d), the battery exhibits a homogeneous surface temperature (compare with Figure 1). This uniform temperature

distribution demonstrates that no temperature gradients along height and circumference direction need to be considered. Consequently, the thermal battery modeling can be reduced to a 1D heat transfer problem in radial direction.
In order to simulate this radial heat transfer numerically with a finite differences method, the battery has to be discretized in radial direction. Figure 7 shows a cylindrical battery, which is discretized equidistantly into N hollow cylinders. Moreover, it illustrates the reduction to one relevant dimension with heat transfer only in radial direction.

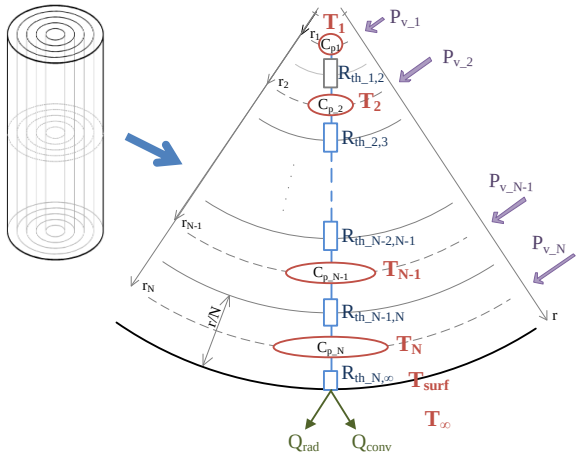

Figure 7: Discretization of a cylindrical battery for finite differences simulation and reduction to a radial 1D heat transfer problem

Each discretization element i consists of an element temperature T_i and a lumped heat capacity C_{p_i}. Neighboring elements are linked by a thermal resistance $R_{th\_i,i+1}$, representing thermal conductivity. Heat exchange with environment comprises radiation Q_{rad} and convection Q_{conv}. Internal heat generation is expressed by irreversible losses P_{v_i}. For our simulations, a discretization with $N = 10$ is used.

2.6.1 Heat Capacity

The heat capacity of the entire battery C_p equals the product of mass m and specific heat capacity c_p of the battery:

$$C_p = m \cdot c_p \tag{8}$$

The lumped heat capacity C_{p_i} of each discretization element with volume V_i is proportional to its ratio of the entire battery volume V ($\pi r^2 h$), where r is the radius and h the height of the battery. For a uniform discretization, the thickness of all hollow cylinders is identical (r/N). This leads to the following volume and heat capacity shares for the discretization elements:

$$V_i = \left(i \cdot \frac{r}{N}\right)^2 \pi h - \left((i-1) \cdot \frac{r}{N}\right)^2 \pi h = \\ = \frac{2i-1}{N^2} r^2 \pi h \tag{9}$$

$$C_{p\_i} = \frac{V_i}{V} \cdot C_p = \frac{2i-1}{N^2} \cdot C_p \tag{10}$$

2.6.2 Heat Conduction

Exchanged heat $Q_{i,i+1}$ between two neighboring discretization elements with lumped heat capacities C_{p_i} and C_{p_i+1} can be expressed by Fourier's law as:

$$Q_{i,i+1} = R_{th\_i,i+1} \cdot (T_i - T_{i+1}) \tag{11}$$

The thermal resistance $R_{th\_i,i+1}$ for the heat flow through the cylinder segment between two neighboring heat capacities is calculated as in [10]:

$$R_{th\_i,i+1} = \frac{\ln(r_{i+1}/r_i)}{\lambda \cdot 2\pi h} \quad \forall\, i \,\epsilon\, [1, N-1] \tag{12}$$

where r_i and r_{i+1} are the inner and outer radii of the heat transfer distance between the two lumped heat capacities. λ is the thermal conductivity of the battery in radial direction.

2.6.3 Heat Exchange with Environment

As the battery exchanges heat with the environment, radiative and convective heat flow are applied to the outermost discretization element. These two boundary conditions depend on the battery's surface temperature T_{surf} and the environment temperature T_∞. T_{surf} is computed based on the thermal resistance $R_{th\_N,\infty}$, which represents the heat conduction through the outer half of the outermost discretization element and is calculated similarly to the other resistances $R_{th\_i,i+1}$ as explained above.
Radiated heat from the battery follows the Stefan-Boltzmann law and is obtained as:

$$Q_{rad} = A_{surf} \cdot \epsilon \cdot \sigma \cdot F \cdot \left(T_{surf}^4 - T_\infty^4\right) \tag{13}$$

where A_{surf} is the battery's surface area ($2\pi rh$), ϵ is the emissivity, σ is the Stefan-Boltzmann constant, and F is the view factor between battery and environment. Since the battery is a convex object in a larger enclosure, F is set to 1. ϵ is assumed to 0.95, as the battery's surface is covered with black insulation tape.
In addition to radiation, heat is also exchanged with environment by natural or forced convection. This additionally emitted heat computes as:

$$Q_{conv} = \alpha_{conv} \cdot A_{surf} \cdot \left(T_{surf} - T_\infty\right) \tag{14}$$

where α_{conv} is the convective heat transfer coefficient, which is assumed to be independent of temperature.

2.6.4 Irreversible Heat Losses

Lastly, the implementation of irreversible losses P_v, used for heating the battery, completes the simulation model. As only inconsiderable temperature gradients occur inside the battery during the applied low-frequency heating currents, losses are assumed to be uniformly distributed inside the cell. Thus, P_{v_i} is proportional to V_i. In analogy to equation (10), P_{v_i} calculates as:

$$P_{v\_i} = \frac{V_i}{V} \cdot P_v = \frac{2i-1}{N^2} \cdot P_v \qquad (15)$$

2.6.5 Transient Thermal Simulation

To simulate transient thermal behavior of the battery, a heat balance is formulated for each discretization element:

$$C_{p\_i} \cdot \dot{T}_i = Q_{i-1,i} - Q_{i,i+1} + P_{v\_i} \quad \forall\, i \in [1, N-1] \qquad (16)$$

$$C_{p\_N} \cdot \dot{T}_N = Q_{N-1,N} + P_{v_N} - Q_{rad} - Q_{conv} \qquad (17)$$

Composing these heat balances for all discretization elements to a system of equations yields:

$$\boldsymbol{C_p} \cdot \dot{T} = \boldsymbol{W_{cond}} \cdot T - Q_{env} + P_v \qquad (18)$$

where T is the vector of all element temperatures, $\boldsymbol{C_p}$ is the diagonal heat capacity matrix, $\boldsymbol{W_{cond}}$ is the heat conduction matrix, vector Q_{env} represents the sum of radiative and convective heat exchange with the environment, and vector P_v contains the generated heat. This equation can now be solved numerically over time and delivers the temperature response of the battery to a specified heating signal.

2.7 Parameter Identification

The implemented battery model is the basis for the identification of thermal cell parameters. With the battery model, TIS measurements are simulated. The same sinusoidal heat excitation as in the experiment is applied to the thermal battery model. Simulation results deliver thermal impedances for each frequency, which form an entire impedance spectrum. The ability to simulate TIS measurements allows rapid creation of impedance spectra for arbitrary thermal cell parameters.

A least-squares optimization routine is employed to systematically adapt the heat capacity, thermal conductivity, and convective heat exchange coefficient of the simulation model until a good agreement between measured and simulated impedance spectra is achieved. Final values of the parameter variation process represent the thermal parameters of the real battery. Figure 8 compares an impedance spectrum from measurement data with an impedance spectrum derived from the result values of the optimization process. As a good agreement between both spectra can be achieved, the utilized battery model is appropriate for thermal parameter identification.

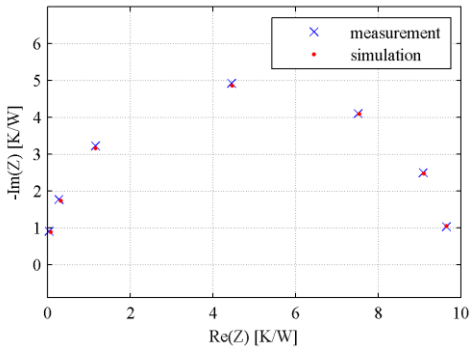

Figure 8: Comparison of thermal impedance spectra from measurement and simulation

3 Measurement Results

Within this article, three cylindrical 18650 Li-ion cells are examined. They are produced by different manufacturers and have different capacities and weights, as listed in Table 2. These cells are chosen to cover a broad spectrum of Li-ion batteries from high energy batteries (cell B) to high power batteries (cell C). Cell A represents a battery type with medial characteristics.

Table 2: Overview of examined cells

Cell	Manufacturer	Capacity	Weight
A	Sanyo	2.0 Ah	42.9 g
B	Panasonic	2.7 Ah	45.0 g
C	A123	1.1 Ah	39.4 g

All measurements are conducted inside a thermal chamber containing a 50 W Peltier element to guarantee constant environmental conditions. Chamber temperature is set to 25 °C and shows fluctuations of less than 0.1 °C. The examined cell is mounted horizontally at the center of the chamber. To obtain the same emissivity for the surfaces of the three examined cells, identical black insulation tape is attached to the cells' surfaces. A PT1000 sensor and a thermocouple are also mounted onto the cell with insulation tape. The thermopile sensor is placed close to the cell in a distance of few millimeters and is facing the cell's surface, which is covered with insulation tape.

The Peltier element in the lid of the thermal chamber contains a heat sink inside and outside the chamber. The fan on the heat sink inside the chamber aspirates air from above the battery and causes turbulence inside the chamber. As this fan is located about 20 cm above the examined cell,

the induced airflow around the cell causes heat exchange by forced convection. The amount of heat exchanged by convection can by varied with the supply voltage of the fan.
Various measurements are performed to investigate the influences of the different temperature sensors, convection and differences among battery types.
For an evaluation of the robustness of the TIS method, parameter identification is performed repeatedly for different sets of excitation frequencies, comprising five to seven frequencies from Table 1. For the reduced sets of frequencies, the lowest frequencies were excluded from evaluation. In the following result chapters, parameter values are always presented in the format $M \pm S$, where M represents the mean value and S is an estimated standard deviation.

3.1 Comparison of Temperature Sensors

For a comparison of sensor technologies, temperature measurements are performed simultaneously with a PT1000 (PT), a thermocouple (TC), and a thermopile (IR) sensor. For this TIS experiment, cell A is employed and fan voltage is set to 12 V. All sensors are calibrated at 20 °C and 30 °C to eliminate effects from miscalibration. As Figure 9 illustrates, the IR sensor shows the highest changes in surface temperature. The contact-based sensors underestimate surface temperatures changes even at low temperature differences to the environment.

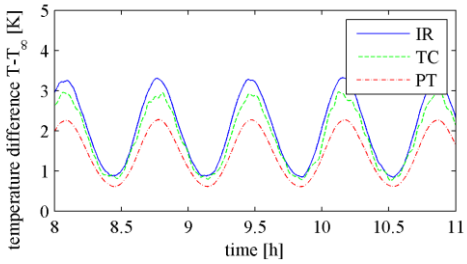

Figure 9: Changes in surface temperature measured with different temperature sensors (cell A, fan 12 V)

Figure 10 depicts the corresponding amplitude and phase shift of the calculated thermal impedances for the applied frequencies. The figure shows that amplitudes diverge pronouncedly in the frequency domain below 0.5 mHz and phase angles diverge at frequencies above 0.5 mHz. The amplitude variations in the low frequency domain lead to different diameters for the semicircles in the Nyquist plot, depicted in Figure 11. The divergence of phase angles leads to negative real parts for the first impedances (> 1 mHz) calculated from PT1000 or thermocouple data.

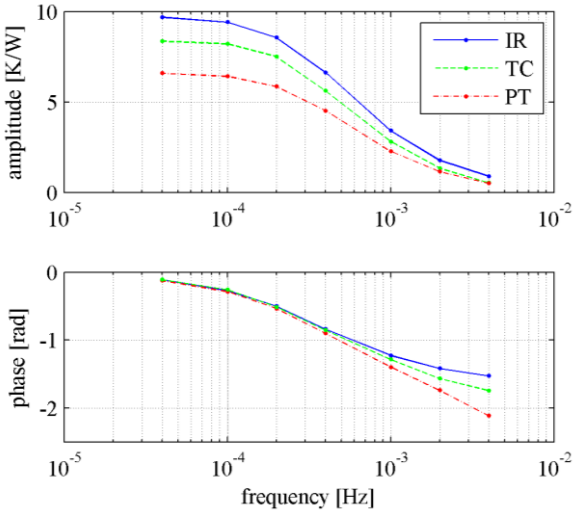

Figure 10: Bode plot of impedances calculated from different sensor data (cell A, fan 12 V)

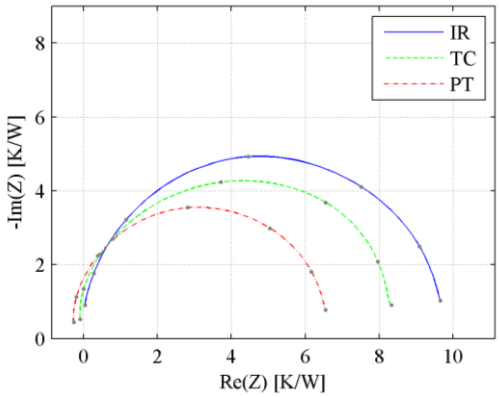

Figure 11: Interpolated Nyquist plot of impedances calculated from different sensor data (cell A, fan 12 V)

As there are substantial differences in impedance spectra for the three temperature sensors, considerable deviations in thermal parameter identification are observed. Thermal parameters for cell A, identified with different sensor data, are shown in Table 3. A comparison of results for heat capacity and convective heat transfer illustrates that TC and PT data yield deviations from IR results which lie in a range of 20 % and 60 %, respectively. Comparing thermal conductivities, deviations from IR results are approximately 30 % and 70 % for the two other sensors.

Table 3: Thermal parameters identified for cell A with measurement data from different sensors (fan 12 V)

Sensor	Heat Capacity [J/kgK]	Thermal Conductivity [W/mK]	Convection [W/m²K]
IR	1013 ± 10	3.09 ± 0.67	21.99 ± 0.07
TC	1212 ± 14	3.95 ± 1.32	25.96 ± 0.18
PT	1601 ± 12	5.34 ± 1.35	33.80 ± 0.66

Table 3 also shows that uncertainty in parameter identification is low for heat capacity and convective heat transfer as the standard deviation is below 1-2 % for all three sensor cases. In contrast, thermal conductivity shows larger deviations, as the standard deviation represents more than 30 %.

3.2 Influence of Convection

As the heat exchange with environment affects the thermal impedance spectrum, the influence of convection on the identified thermal parameters is investigated. This series of measurements also provides information about the reliability of the TIS method. As only convection is changed but not the cell itself, the values calculated for heat capacity and thermal conductivity have to remain constant. For this series of experiments, cell B is employed. Temperature measurement is performed with the IR sensor system and fan voltage is varied from 0 V (fan off) to 16 V.

The influence of convective heat exchange on the amplitude and phase of the thermal impedance is illustrated in Figure 12. For frequencies above 1 mHz, the amplitudes show no difference. For frequencies below 1 mHz, amplitudes diverge: the lower the convective heat exchange, the higher the amplitude. The phase curves show distinct separation between 0.1 mHz and 1 mHz. For frequencies below and above this interval, phase values converge.

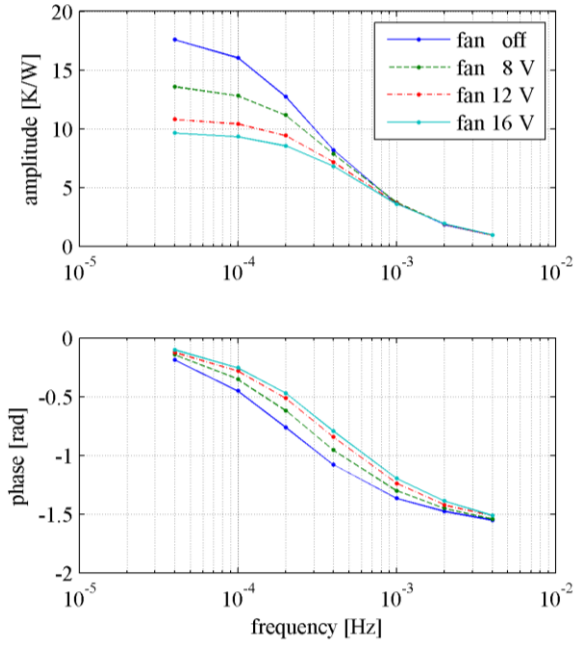

Figure 12: Bode plot for TIS measurements at different rates of convection (cell B, IR sensor)

In the Nyquist plot (Figure 13), the differences in amplitude become visible in the form of different diameters of the depicted semicircles.

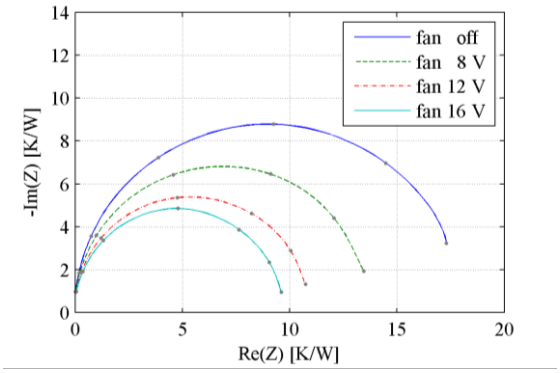

Figure 13: Interpolated Nyquist plot for TIS measurements at different rates of convection (cell B, IR sensor)

Explicit values for the heat capacity, thermal conductivity and convective heat exchange are provided in Table 4. The different supply voltages for the fan between 8 and 16 V lead to specific heat capacities that are close together and show deviations of less than 1 %. The heat capacity for "fan off" is almost 4 % higher than the other values. This is caused by the deactivated Peltier element. Thus, temperature inside the test chamber does not remain constant and distorts parameter identification. Thermal conductivity shows larger deviations, but stays at an order of 3.5 W/mK.

Table 4: Thermal parameters of cell B, calculated from TIS measurements with different rates of convection

Fan	Heat Capacity [J/kgK]	Thermal Conductivity [W/mK]	Convection [W/m²K]
off	941 ± 7	3.05 ± 0.68	9.53 ± 0.14
8 V	907 ± 7	3.48 ± 1.26	14.11 ± 0.03
12 V	910 ± 6	3.94 ± 2.14	19.28 ± 0.05
16 V	907 ± 6	3.59 ± 0.30	22.46 ± 0.05

3.3 Comparison of Battery Types

Cylindrical 18650 Li-ion cells with high energy and high power characteristics often contain different cell chemistries and have a different cell design with regard to electrode thicknesses [11]. To investigate influences of the battery type on thermal parameters, TIS measurements are performed with three different 18650 cells. For comparison, data with equivalent convective boundary conditions are selected. Table 5 shows the results of thermal parameter identification. Heat capacity values show that the high energy battery (cell B) examined has a heat capacity about 10 % lower than the other two cells. Thermal conductivity lies

in the same range for all cells. More specific conclusions for conductivity cannot be drawn owing to higher uncertainties in parameter identification.

Table 5: Thermal parameters calculated for different cell types (IR temperature measurements)

Cell	Heat Capacity [J/kgK]	Thermal Conductivity [W/mK]	Convection [W/m²K]
A	1013 ± 10	3.09 ± 0.67	21.99 ± 0.07
B	907 ± 6	3.59 ± 0.30	22.46 ± 0.05
C	1011 ± 5	3.61 ± 1.28	21.04 ± 0.07

4 Discussion

To evaluate the quality of results obtained from TIS measurements with an IR-based sensor system, thermal parameters are compared with reference values from the literature. Maleki et al. [2] examined a cylindrical 18650 Li-ion cell from Sony. They determined a specific heat capacity of about 1000 J/kgK and a cross-plane thermal conductivity of 3.4 W/mK for a stack of positive electrode, separator, and negative electrode soaked with electrolyte. These values confirm the results of our TIS measurements performed with the IR sensor system, which yields heat capacities between 900 and 1020 J/kgK. Moreover, our derived thermal conductivities range between 3.1 and 3.6 W/mK and are in good agreement with the data presented in the literature.

Furthermore, our measurements demonstrate that contact-based temperature sensors are not efficient at measuring surface temperatures. Taking the sensor temperature as the value for the battery's surface temperature leads to an underestimation of the battery temperature. This causes a substantial overestimation of heat capacity as well as convective heat exchange of about 20 % for thermocouples and 60 % for the PT1000 thermistors in our experimental setup. Consequently, these temperature measurements cannot be used for reliable thermal parameter identification.

These findings can explain several discrepancies mentioned in the TIS literature. In [3], a substantial overestimation of heat capacity and convective heat exchange is reported. For heat capacity, they yield a value which was almost 80 % higher than a reference value obtained from calorimetric studies. With regard to our comparison of different temperature sensors (see Table 3), this effect can be explained by errors in temperature measurement typical for contact-based temperature sensors.

In [4], no validation of the TIS method was performed. Thus, no statement on accuracy is given. The third TIS reference [5] takes a time delay of the thermocouple into account. However, they also report a difference in heat capacity of about 5 % compared to a reference value from calorimetry. As the time delay approach considers no heat exchange of the sensor with the environment, there is still an underestimation of the battery's surface temperature. Regarding Bode plots, such as Figure 10 and Figure 12, it becomes obvious that inserting a time delay for the sensor can only correct errors in phase but not in amplitude. Hence, the errors presented in this reference might also be related to errors in temperature measurement.

The repeated TIS measurements at different rates of convection demonstrate the importance of constant environment temperature for TIS measurements. The values of estimated standard deviation from several evaluation runs show that a stable data evaluation with good repeat accuracy is obtained for heat capacity and heat exchange with the environment. Thermal conductivity, however, shows higher deviations, which require an averaging of several evaluation runs to achieve reliable values. The deviations may be related to uncertainties in the phase value obtained from the curve fitting process. Overall, the measurements show that IR temperature data leads to lower uncertainties in parameter identification compared to thermocouple and PT1000 data.

5 Conclusion

Our investigations show that IR-based temperature sensors are an effective progression for TIS measurements and improve quality of parameter identification at low cost. Moreover, discrepancies between thermal parameters obtained by TIS measurement and calorimetry results mentioned in the TIS literature can be explained by our investigations.

The heat capacity of Li-ion batteries and heat exchange with the environment can be determined reliably owing to a high repeat accuracy. The specific heat capacities identified for three different cells range between 900 and 1020 J/kgK, which is in good agreement with literature data. Thermal conductivity is determined in a range between 3.1 and 3.6 W/mK. This is also in good accordance with the literature but results exhibit larger deviations.

These deviations could be reduced by improved excitation signals and optimized curve fitting routines. Selecting the right offset current, current amplitude, and repetition per frequency may im-

prove signal-to-noise ratio for frequencies above 1 mHz. This leads to more accurate curve fitting results which are the basis for reduced deviations in thermal conductivity.
Another focus of further work is an acceleration of TIS measurements. We are currently investigating methods for reducing measurement time to only a few hours. This acceleration is necessary to establish TIS as a practicable method for thermal parameter identification for larger numbers of cells.

Acknowledgments

The authors like to thank the German Federal Ministry of Education and Research for their financial support.

References

[1] T. M. Bandhauer et al., *A Critical Review of Thermal Issues on Lithium-Ion Batteries*, Journal of the Electrochemical Society, ISSN 0013-4651, 158(2011), R1-R25.

[2] H. Maleki et al., *Thermal Properties of Lithium-Ion Battery and Components*, Journal of the Electrochemical Society, ISSN 0013-4651, 146(1999), 947-954.

[3] E. Barsoukov et al., *Thermal impedance spectroscopy for Li-ion batteries using heat-pulse response analysis*, Journal of Power Sources, ISSN 0378-7753, 109(2002), 313-320.

[4] J. P. Schmidt et al., *Investigation of the ther-thermal properties of a Li-ion pouch-cell by electrothermal impedance spectroscopy*, Journal of Power Sources, ISSN 0378-7753, 196(2011), 8140-8146.

[5] M. Fleckenstein et al., *Thermal Impedance Spectroscopy - A method for the thermal characterization of high power battery cells*, Journal of Power Sources, ISSN 0378-7753, 223(2013), 259-267.

[6] J. Fraden, *Handbook of modern sensors: physics, design, and application*, 3rd ed., ISBN 0-397-00750-4, New York, Springer-Verlag, 2004, 457-461.

[7] J. R. Macdonald, *Impedance Spectroscopy*, Annals of Biomedical Engineering, ISSN 0090-6964, 20(1992), 289-305.

[8] E. Barsoukov, J. R. Macdonald, *Impedance Spectroscopy: Theory, Experiment, and Applications*, 2nd ed., ISBN 0-471-64749-7, New Jersey, John Wiley & Sons, 2005.

[9] V. V. Viswanathan et al., *Effect of entropy change of lithium intercalation in cathodes and anodes on Li-ion battery thermal management*, Journal of Power Sources, ISSN 0378-7753, 195(2010), 3720-3729

[10] F. Kreith et al., *Principles of Heat Transfer*, 7th ed., ISBN 0-495-66770-6, Stanford, Cengage Learning, 2011.

[11] H. Zheng et al., *A comprehensive understanding of electrode thickness effects on the electrochemical performances of Li-ion battery electrodes*, Electrochimica Acta, ISSN 0013-4686, 71(2013), 258-265.

Authors

Dipl.-Ing. Peter Keil
earned his diploma degree in mechanical engineering from TU Munich in 2010. Currently, he is working as a research associate and team leader at the institute for Electrical Energy Storage Technology, TU Munich. His main research activities are in the field of electrical and thermal characterization of Li-ion batteries.

Dipl.-Geophy. Katharina Rumpf
earned her diploma degree in Geophysics from CAU Kiel in 2012. She is currently working as a research associate at the Institute for Electrical Energy Storage Technology, TU Munich. Her main research activities comprise thermal modeling of Li-ion battery cells and systems.

Prof. Dr.-Ing. Andreas Jossen
is full professor at the Institute for Electrical Energy Storage Technology, TU Munich, since 2010. He earned his doctorate, dealing with 'Management of photovoltaic plants using energy storage systems', at University of Stuttgart. From 1994 he was group leader for different battery related topics with ZSW, Ulm.